Microexplosion in Burning Emulsified Fuel Droplets

Saroj Ray[a,*], Song Cheng[b,*]

[a] Department of Mechanical Engineering, National Institute of Technology Rourkela, India

[b] Department of Mechanical Engineering, The Hong Kong Polytechnic University, Hung Hom, Kowloon, Hong Kong

* Corresponding authors:

Saroj Ray, rays@nitrkl.ac.in

Song Cheng, songryan.cheng@polyu.edu.hk

Abstract:

This paper presents an analytical model for simulating microexplosions in burning emulsified fuel droplets. A key feature of the proposed model is its ability to capture bubble growth within a droplet, which triggers microexplosions, while also incorporating the effects of droplet combustion. The model offers a comprehensive formulation for a single bubble inside a burning droplet, accounting for bubble dynamics, heat transfer, phase change, and combustion processes. The methodology outlining the mathematical framework, governing equations, and underlying assumptions are presented. The model is applied specifically to n-dodecane/water emulsion droplets, and the results are analyzed in detail and validated against experimental data from previous studies. The evolution of the bubble radius reveals two distinct growth stages: an initial thermally controlled phase followed by an inertially controlled phase. Droplet growth also proceeds in two stages – initially independent of bubble growth, and later becoming interdependent. Notably, the microexplosion delay time decreases gradually with increasing initial bubble radius but increases sharply with a larger initial droplet radius. The developed analytical model has the potential for simulating spray combustion of water-emulsified fuels with significantly reduced computational cost while maintaining sufficient fidelity.

Keywords: Microexplosion, bubble dynamics, droplet heating, droplet combustion.

1. Introduction

The efficient and clean combustion of fuels is of paramount concern in various industrial applications, particularly in spray combustion devices and internal combustion (IC) engines. The growing demand for energy coupled with stringent environmental regulations necessitates the exploration of innovative fuel technologies. Emulsified fuels have emerged as a promising alternative, demonstrating significant benefits in mitigating both particulate matter and nitrogen oxides (NOx) emissions simultaneously [1]. The implementation of water-in-diesel emulsion fuel in diesel engines, for instance, has been shown to reduce NOx emissions due to the water content lowering the adiabatic flame temperature. Furthermore, these emulsions effectively suppress particulate matter formation, largely because fuel evaporation and fuel/air mixing are significantly enhanced by the phenomenon of microexplosion in fuel droplets [2, 3]. For highly viscous fuels, such as biodiesel, which typically produce larger droplets in IC engines leading to incomplete combustion and longer combustion times, the use of biodiesel-water emulsified fuels has proven to overcome this issue by facilitating the production of finer droplets through microexplosions [4]. Beyond emulsified fuels, several other methods have been proposed and investigated to lower IC engine emissions, including the addition of nanoparticles, or alcohols to fuels [5, 6].

Microexplosion is defined as the violent breakdown of multicomponent fuel droplets. The earliest foundational research on microexplosion in burning two-component fuel droplets was conducted by Ivanov and Nefedov [7], who discovered that the incorporation of water into fuel significantly improves combustion efficiency due to faster water evaporation that leads to a direct consequence of microexplosion. The rapid, explosive breakdown associated with microexplosion leads to a superior mixing of fuel vapour with the surrounding ambient gas [8]. Consequently, microexplosion in emulsified fuels acts as a mechanism for secondary atomization, producing much finer droplets. This process inherently increases the surface-to-volume ratio of the fuel, thereby enhancing the overall evaporation rate.

The phenomenon of microexplosion in multicomponent droplets has been investigated experimentally using various techniques, including suspended droplets, falling droplets, and Leidenfrost methods [9-13]. In many of these studies, droplet combustion occurs at elevated ambient temperatures. Watanabe et al. [11] experimentally studied the puffing of kerosene/water emulsion saturated with carbon dioxide. They observed that the addition of carbon dioxide in the emulsified fuel droplets reduces the time to puffing as the dissolved carbon dioxide reduces the nucleation energy of bubbles. Morozumi and Saito [12] experimentally investigated the influence of an emulsifier on microexplosion of n-

hexadecane/water droplets. They found that microexplosion delay time (defined as the time taken for the onset of a breakdown of emulsified droplet into finer droplets under heating or burning conditions) increase with increasing emulsifier content. A comparative study on microexplosion of sunflower oil/water emulsion with varying surfactant content by employing two experimental techniques -suspended droplet and Leidenfrost techniques was carried out by Mura et al. [13]. A small Type-K thermocouple (76.2 μm in diameter) was used as a suspender in the suspended droplet technique, and also in the Leidentfrost technique to measure the droplet temperature. They argued that the presence of a suspender did not cause noticeable differences between the results obtained from the two experimental techniques. Califano et al. [14] experimentally investigated the effect of emulsion stability on microexplosion for diesel/water droplets, and reported that stability of emulsion has a noticeable effect on microexplosion. Khan et al. [15] experimentally investigated microexplosion in water-in-diesel emulsion using the Leidenfrost technique. They concluded that the size of secondary droplets (which can undergo further microexplosion) formed from microexplosion is slightly influenced by the initial droplets size. Rao et al. [16-17] concluded that bubble growth can occur through the merging of two bubbles to form a larger bubble. They also observed that during droplet breakup, ligaments are formed, and the breakup can occur at either the ligament tip or base, leading to the formation of secondary droplets. Avulapati et al. [18] classified microexplosions into two categories: strong and weak. A strong microexplosion is caused by a single nucleus (or vapor bubble) located near the droplet center, while multiple nuclei result in a weak microexplosion, producing slightly coarser child droplets. Stodt et al. [19] found that the parent droplets can undergo a rotational motion due to the asymmetric expulsion of secondary droplets occurring during microexplosion. While the microexplosion of burning emulsified droplets has been explored experimentally, a comprehensive model for this process has not been developed.

The modeling of microexplosion in droplets without combustion has been pursued for many years, particularly through the use of computational fluid dynamics (CFD) models. A robust CFD model designed to simulate microexplosion in droplets should encompass several key processes, including droplet heating, bubble nucleation, bubble growth, and droplet breakup. Law [8] analyzed the onset of nucleation inside a multicomponent droplet. A CFD model based on transient heat and mass diffusion inside the droplet, quasi-steady transport in the gas phase, and ideal behavior for the mixture was employed. Law concluded that the presence of volatile components inside rapidly heating multicomponent droplets can cause nucleation and ultimately lead to violent breakdown due to internal pressure build-up. A

linear instability analysis was performed by Zeng and Lee [20] to analyze the breakup of droplets with a bubble present at the droplet center. Shinjo et al. [21-23] developed a comprehensive CFD model for microexplosion and puffing. Their model considered a water sub-droplet inside the fuel droplet, and a bubble inside the sub-droplet. Navier-Stokes equation, energy balance equations, and species balance equations were solved, where they found that detachment took shorter time for smaller water sub-droplet, and the fuel droplet breakup happened in a localized area, and became more violent for large water sub-droplet located near the droplet center. They did not compare their numerical results against any experimental data. Guida et al. [24] revealed that the bubble-to-droplet size ratio notably affects the droplet disintegration. Their model predicted the breakup times that agree well with the experimental data. In general, the CFD model developed in previous studies considers transient droplet heating, and the present of one or two bubbles in the droplet, as well as bubble growth. These models are, however, computationally expensive to apply in practical spray combustion modeling where microexplosion of millions of droplets take place simultaneously.

To overcome the substantial computational cost associated with CFD models, reasonably simplified analytical models, supported by justified assumptions, offer a viable alternative. A common approach in analytical models for microexplosion in a droplet involves solving the heat diffusion equation [25-27]. Additionally, a criterion based on the boiling point of the volatile component is often employed to determine the microexplosion delay time [25].

A simple analytical model of microexplosion was proposed by Sazhin et al. [25], in which they assumed that a water sub-droplet is located at the center of the droplet. Their criterion for determining the microexplosion time was based on the duration required for the water-fuel surface to reach the boiling point of water. In a subsequent study, they replaced the boiling point with the nucleation temperature and introduced a bubble at the water-fuel surface at this temperature [28]. Their criterion for microexplosion was defined as the moment when the bubble size reaches twice the initial droplet diameter [29]. Later, their research group extended this model to two- and three-droplet systems, accounting for the influence of nearby droplets using a Nusselt number correlation [30-31]. While this model is straightforward and adequately explains the experimental data, the assumption that all the water is concentrated at the center of the droplet represents an extreme case. In reality, water can be distributed throughout the entire volume of the emulsified droplet.

The model proposed by Ray et al. [32] takes a different approach by assuming that water is uniformly distributed throughout the droplet, with a bubble located at the center of the multicomponent droplet. They consider the average properties of the droplet based on the composition of water and fuel, and they also account for multiple bubbles within the droplet that quickly merge to form a single larger bubble. However, their model does not address the combustion of the droplet. In this study, we focus on a bubble within a burning droplet. Earlier research by the authors group [32] demonstrated the merging of multiple bubbles into a single bubble, thus, growth of a single bubble in a droplet is considered in this paper.

A novel analytical model for microexplosion in a burning droplet is proposed in this study. The significant novelties of this proposed model are twofold: (1) it explicitly considers bubble growth inside a droplet, which is the precursor to microexplosion, and (2) it integrates the combustion of the droplet into the model, aspects that were neglected in many previous studies. In an emulsified fuel, the process of microexplosion is initiated by heterogeneous nucleation, leading to the formation of bubbles inside the droplet, which subsequently grow, merge, and ultimately trigger the onset of microexplosion. Therefore, the primary motivation for the present study is to develop a robust analytical model for the microexplosion of a burning emulsified fuel droplet, a model that systematically includes bubble growth, heat transfer, phase change, and combustion. The formulation for a single bubble within a burning droplet is rigorously developed and its results are thoroughly analyzed and validated.

The subsequent sections of this paper are organized as follows: Section 2 presents the analytical model developed in this study, including the governing equations and underlying assumptions of the model. Section 3 details the solution methodology implemented for analysing microexplosion in n-dodecane/water emulsion droplets. Section 4 provides the validation of the model against experimental data from previous studies and discusses the effect of various parameters on microexplosion delay time along with the dynamics of the bubble growth, the droplet growth, and flame location is thoroughly analyzed. Finally, Section 5 summarises the important conclusions derived from this study.

2. Description of Analytical Model

The theoretical model considered a stationary liquid droplet containing a bubble within a hot and quiescent ambient environment. In this scenario, the initial size of the bubbles is significantly smaller than that of the droplet itself. As the droplet-bubble system is subjected to transient heating from the surrounding hot gas, the bubbles have the potential to expand radially in response to the increased thermal energy. As the droplet absorbs heat, it

may begin to undergo combustion, leading to a regression of its surface due to evaporation. This process not only affects the droplet's size but also influences the dynamics of the bubbles within it. The interaction between the heat transfer, bubble expansion, and droplet combustion creates a complex interplay of physical phenomena that can significantly impact the overall behavior of the system.

To illustrate this model, a schematic representation for the case involving a single bubble is provided in Fig. 1. In Fig. 1b, δ represents the minimum thickness of the liquid layer, defined as the distance between the bubble surface and the droplet surface. This diagram highlights the key components of the model, including the droplet, the bubble, the flame, and the surrounding ambient conditions, thereby offering a visual understanding of the processes at play in this theoretical framework.

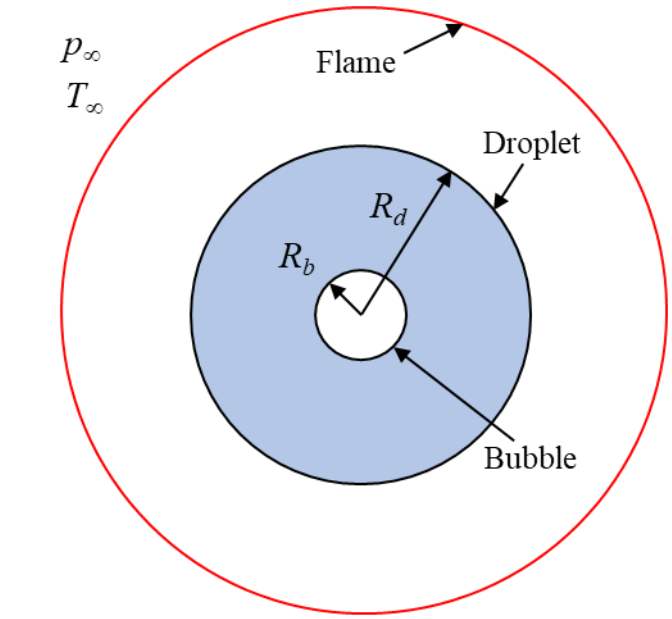

(a)

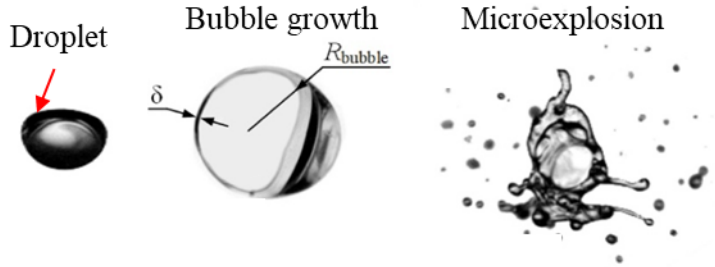

(b)

Figure 1. (a) Schematic of a bubble inside a burning droplet in a quiescent ambient at temperature of T_∞ and pressure of p_∞, and (b) images showing sequences of microexplosion in 90% rapeseed and 10% water droplet (T_∞ = 1223 K, D_{d0} = 1.680 mm) [33].

2.1 Bubble growth inside a droplet

The dynamics of bubble growth within the droplet are described by an ordinary differential equation (ODE) derived by Ray et al. [32]. This equation is formulated by solving the principles of mass conservation and momentum conservation in the liquid region of the droplet. Two boundary conditions: one at the interface between the bubble and the droplet, and the other at the surface of the droplet itself has been applied. This governing equation effectively captures the behavior of bubble growth in relation to the surrounding droplet environment and is expressed as follows:

$$\frac{p_b - p_\infty}{\rho_l} = R_b \frac{d^2 R_b}{dt^2} + \frac{3}{2}\left(\frac{dR_b}{dt}\right)^2 + \frac{4\mu_l}{\rho_l R_b}\frac{dR_b}{dt} + \frac{2\gamma}{\rho_l R_b} + \frac{2\gamma}{\rho_l R_d}. \quad (1)$$

where p, R, μ, and γ represent the pressure, radius, dynamic viscosity, and surface tension, respectively. The subscripts *b*, *d* and ∞ denote the bubble, droplet, and ambient conditions, respectively. This equation (i.e., equation (1)) is a fundamental component of the theoretical model, offering valuable insights into the complex processes that occur within the droplet during heating and combustion. Equation (1) is a modified form of the Rayleigh-Plesset equation [34-35], which describes bubble growth over time in an infinite pool of liquid. The original Rayleigh-Plesset equation was first derived by Lord Rayleigh [34] under inviscid isothermal conditions. It was later extended and applied to bubble expansion in superheated liquids by Plesset and Zwick [34], as well as by Mikic et al. [36]. This evolution of the equation allows for a more comprehensive understanding of bubble dynamics in various thermal environments.

The bubble initially contains a small amount of gas and also accumulates liquid vapor due to phase change occurring at the bubble surface. Assuming that the initial gas does not diffuse into the liquid, the gas pressure (p_g) at a later time is determined by

$$p_g = p_{g0}\left(\frac{R_{b0}}{R_b}\right)^{3\gamma}, \quad (2)$$

where p_{g0}, R_b, R_{b0}, and γ are the initial gas pressure, bubble radius, initial bubble radius, and ratio of specific heat of gas, respectively. The initial gas pressure is calculated using the ideal gas equation of state

$$p_{g0} = \frac{n_a R_u T_b}{V_0}, \tag{3}$$

where n_a is the number of moles of gas present in the bubble, R_u is the universal gas constant, T_b is the bubble temperature, and $V_0 = \frac{4}{3}\pi R_b^3$ is the initial volume of the bubble. The total pressure (p_b) inside the bubble is the sum of the vapour pressure (p_v) and the gas pressure (p_g),

$$p_b = p_v + p_g . \tag{4}$$

The vapor pressure inside the bubble is calculated by Antoine equation [37] which related the temperature at the bubble-droplet interface to the vapor pressure and expressed as,

$$\log_{10} p_v = A - \frac{B}{T + C}, \tag{5}$$

where A, B, and C are constant coefficient.

2.2 Heat transfer in the droplet with a bubble

The liquid inside the droplet is assumed to be a Newtonian fluid [38], with the flow being radially outward (one-dimensional) and the liquid density remaining constant. Under these assumptions, the conservation of mass inside the droplet is expressed as

$$\frac{\partial\left(r^2 u\right)}{\partial r} = 0, \tag{6}$$

where r is the radial position and u is the radial component of velocity inside the droplet, respectively. Upon integration in the liquid phase, Equation (6) can be written as

$$r^2 u = R_b^2 \frac{dR_b}{dt} = F\left(t\right), \tag{7}$$

where R_b is the bubble radius at time t, and $F(t)$ is the constant of integration that can vary with time.

Droplet heating is governed by a one-dimensional transient heat equation in spherical coordinates [39], incorporating convection effects and can be expressed as

$$\frac{\partial T}{\partial t} + u\frac{\partial T}{\partial r} = \alpha \frac{\partial}{\partial r}\left(r^2 \frac{\partial T}{\partial r}\right), \tag{8}$$

where T, and α are the temperature and the thermal diffusivity, respectively. By substituting the expression for u (i.e., $u = \frac{R_b^2}{r^2}\frac{dR_b}{dt}$), the partial differential equation governing heat transfer in a spherical shell is given by,

$$\frac{\partial T}{\partial t} + \left(\frac{R_b}{r}\right)^2 \frac{dR_b}{dt}\frac{\partial T}{\partial r} = \alpha \frac{1}{r^2}\frac{\partial}{\partial r}\left(r^2 \frac{\partial T}{\partial r}\right) \tag{9}$$

The boundary conditions applied to this heat transfer model are

$$r = R_b: \left.\frac{\partial T}{\partial r}\right|_{r=R_b} = \frac{L\rho_v}{k}\frac{dR_b}{dt},$$

and

$$r = R_d: \quad T(r, t) = T_d, \text{ where } r \in [R_b, R_d].$$

The initial condition is

$$t = 0: \quad T(r, 0) = T_d.$$

Here, α, L, ρ_v, k, and T_d are thermal diffusivity, latent heat of vaporization, vapor density inside the bubble, thermal conductivity of the liquid phase, and the droplet surface temperature, respectively. Under steady-state $\frac{\partial T}{\partial t} \approx 0$, equation (9) becomes an ordinary differential equation (ODE) which can be written as,

$$\left(\frac{R_b}{r}\right)^2 \frac{dR_b}{dt}\frac{dT}{dr} = \alpha \frac{1}{r^2}\frac{d}{dr}\left(r^2 \frac{dT}{dr}\right) \tag{10}$$

We assume that the solution of equation (10) is of the form,

$$T(r,t) = T_d + C\left(\frac{1}{r} - \frac{1}{R_d}\right). \tag{11}$$

Applying the boundary condition at $r = R_d$ in equation (11) gives $T(R_d,t) = T_d$, which satisfy the boundary condition. Applying the flux condition at $r = R_b$,

$$\frac{dT}{dr} = -C\left(\frac{1}{r^2}\right), \text{ so} \tag{12}$$

$$\left.\frac{dT}{dr}\right|_{r=R_b} = -C\left(\frac{1}{R_b^2}\right). \tag{13}$$

Substituting this into the flux boundary condition at $r = R_b$ yields

$$\left.\frac{\partial T}{\partial r}\right|_{r=R_b} = \frac{L\rho_v}{k}\frac{dR_b}{dt} = -C\left(\frac{1}{R_b^2}\right), \tag{14}$$

from which C is obtained as

$$C = -R_b^2 \frac{L\rho_v}{k} \frac{dR_b}{dt}. \tag{15}$$

Thus, the analytical solution describing the steady-state temperature distribution is expressed as

$$T(r,t) = T_\infty - \left(\frac{1}{r} - \frac{1}{R_d} \right) R_b^2 \frac{L\rho_v}{k} \frac{dR_b}{dt}. \tag{16}$$

The density of the bubble (ρ_b) is calculated using the ideal gas law,

$$\rho_b = \frac{p_b V_b}{R_g T_b}, \tag{17}$$

where $R_g = \frac{R_u}{MW}$ is the gas constant, R_u is the universal gas constant, MW is the molecular weight, and V_b is the bubble volume, respectively.

2.3 Droplet combustion sub-model

A droplet combustion sub-model is integrated into the overall analytical framework. This subsection presents several equations pertinent to the sub-model, which are crucial for understanding the burning behavior of the droplet. A detailed derivation of the sub-model can be found in Ref. [40]. The combustion process of the droplet generates a spherically symmetric diffusion flame at a distance r_f from the droplet center, enveloping the droplet. At the flame, fuel and air react instantaneously in a stoichiometric proportion, which is represented by a thin sheet.

Equation (18) provides an expression for the mass burning rate ($\dot{m}_F$) in terms of the flame radius (r_f) and the mass transfer number ($B_{o,q}$),

$$\dot{m}_F = \frac{4\pi k_g R_d}{c_{pg}} \ln\left(1 + B_{o,q}\right). \tag{18}$$

where, k_g is the gas phase thermal conductivity, and c_{pg} is the gas phase specific heat capacity at constant pressure. The mass transfer number is given by

$$B_{o,q} = \frac{\Delta h_c / \nu + c_{pg}\left(T_\infty - T_d\right)}{q_{i-l} + h_{fg}}, \tag{19}$$

where, Δh_c, ν, h_{fg}, and q_{i-l} is the heat of combustion, the stoichiometric air-fuel ratio, latent heat of vaporization, and heat transfer from gas to liquid at the droplet surface, respectively. The flame temperature (T_f) is determined by

$$T_f = \frac{q_{i-l} + h_{fg}}{c_{pg}\left(1+\nu\right)}\left[\nu B_{o,q} - 1\right] + T_s\,, \tag{20}$$

The flame radius (r_f) itself is related to the droplet radius and the mass transfer number,

$$r_f = R_d \frac{\ln\left[1 + B_{o,q}\right]}{\ln\left[\left(\nu+1\right)/\nu\right]}\,. \tag{21}$$

The fuel mass fraction at the droplet surface ($Y_{F,s}$) is given by

$$Y_{F,s} = \frac{B_{o,q} - 1/\nu}{B_{o,q} + 1}\,, \tag{22}$$

Finally, the droplet surface temperature (T_s) is calculated by using the Clausius-Clapeyron equation and expressed as

$$T_s = \frac{-D}{\ln\left[\dfrac{-Y_{F,s}P_\infty MW_{\mathrm{Pr}}}{E\left(Y_{F,s}MW_F - Y_{F,s}MW_{\mathrm{Pr}} - MW_F\right)}\right]}\,. \tag{23}$$

where D and E are constants estimated using the Clausius-Clapeyron equation. The variables Y, P, and MW represent the mass fraction, pressure, and molecular weight, respectively. The subscripts F, s, Pr, and ∞ denote the fuel, droplet surface, product, and ambient conditions.

These detailed formulations for bubble growth, heat transfer, and droplet combustion collectively form the analytical model developed in this study, aiming to provide a comprehensive understanding of microexplosion in burning emulsified fuel droplets.

3. Model Specification

The model developed in Section 2 is applied to simulate microexplosion in a system consisting of n-dodecane and water droplets. To begin, the bubble growth rate (dR_b/dt) is determined by solving Equation (1). The heat flux at the bubble surface, which is necessary for the boundary condition, is calculated using the temperature profile provided in Equation (16). Additionally, the droplet combustion sub-model is employed to assess various parameters, including the mass burning rate, flame temperature, flame radius, and droplet surface temperature. Several criteria have been proposed to determine the microexplosion delay time. Ray et al. [32] considered the time taken for the bubble to reach the droplet surface, accounting for the buoyancy-driven motion of the bubble. Other criteria used in previous research include the time taken for the bubble to expand to the initial droplet radius [27] or to twice the initial radius [29]. In this study, to maintain the spherical symmetry of the

model, we have adopted the criterion of the time taken for the bubble radius to reach twice the initial radius. In the present study, the initial bubble is assumed to be located at the center of the droplet. Although the model can be extended to account for off-center bubble positions by following the procedure outlined in the authors' previous work on non-combusting droplet microexplosions (see Ray et al., 2023), doing so would significantly increase the model's complexity. Similarly, while a non-spherical droplet shape can influence microexplosion behavior, incorporating such geometry would further complicate the analytical formulation. Therefore, a spherical droplet shape is considered for simplicity.

In emulsified fuels, heterogeneous nucleation is a complex process that generates numerous tiny bubbles dispersed within a droplet. These bubbles grow and eventually coalesce to form larger bubbles. To simplify the modeling, a single bubble with a representative size is considered to capture the effects of heterogeneous nucleation. This approach eliminates the need to model the bubble coalescence process. The model accurately accounts for bubble growth, heat transfer, phase change, and combustion. The breakup of a droplet during a microexplosion is a highly complex phenomenon that typically requires computationally intensive fluid dynamics simulations. However, because the breakup occurs over a much shorter time scale than the microexplosion delay time, this study adopts a simplified criterion for predicting the onset of microexplosion.

For this simulation, the initial droplet is assumed to contain 15% water and 85% n-dodecane by volume, with a uniform initial temperature of 300 K. The droplet is surrounded by ambient air, which also maintains a uniform initial temperature of 300 K. The bubble within the droplet consists of a small amount of air and water vapor, sharing the same initial temperature as the droplet. The initial properties of the liquid phase in the droplet, which is a mixture of water and n-dodecane, are determined using linear mixing rules. The transport properties of individual component and mixture are estimated by the methodology mentioned in Ray et al. [32].

An in-house Python-based code has been developed to perform these calculations. A timestep of 0.1 μs is chosen for the analysis, as it effectively captures the dynamic behavior of microexplosion phenomena while balancing accuracy and computational efficiency. With this configuration, each simulation completes within 1 minute on a 3.2 GHz, 4-core processor with 16 GB of memory.

4. Results and discussion

4.1 Comparison with experiments

To validate the developed model, we first examined the microexplosion of an evaporating droplet. For this case, a single bubble positioned at the center of the droplet, with its initial diameter being at least an order of magnitude smaller than that of the droplet. The model predictions are compared with experimental data from Sazhin et al. [25]. The initial droplet diameters ranged from 50 μm to 175 μm, while the initial bubble diameter was consistently set at 2 μm. The microexplosion delay time for the 50 μm droplet (denoted as t^*) was used to normalize both theoretical and experimental data. The ambient conditions were maintained at 700 K and 1 atm, matching those in the referenced experiments.

Figure 2 illustrates the relationship between the microexplosion delay time (t_e) and the initial droplet diameter. It is evident that the delay time increases as the droplet diameter increases. The model predictions align well with the experimental data [25], indicating that the model is able to accurately capture microexplosion processes. To enhance the reliability of the proposed model, its predictions are further compared with experimental data and theoretical results from Nissar et al. [26]. The root mean square errors between the model predictions and literature data are 8.2% and 6.5% for Fig. 2 and Fig. 3, respectively. It should be noted that the models proposed by Sazhin et al. [25] and Nissar et al. [26] are based on non-combustion scenarios.

4.2 Microexplosion of evaporating droplet

To gain deeper insights, we further analyzed the microexplosion under evaporation conditions, focusing on the effects of both the initial droplet radius and the initial bubble radius.

The evolution of the bubble and droplet radii was systematically studied. As shown in Figure 4(a), the bubble radius increases steadily over time, with a more rapid growth observed in the initial phase ($t < 0.05$ ms), followed by a linear increase. Figure 4(b) depicts the rate of change of the bubble radius over time, revealing two distinct growth phases: a rapid growth phase with a steep slope ($t < 0.05$ ms) and a slower growth phase ($t > 0.2$ ms).

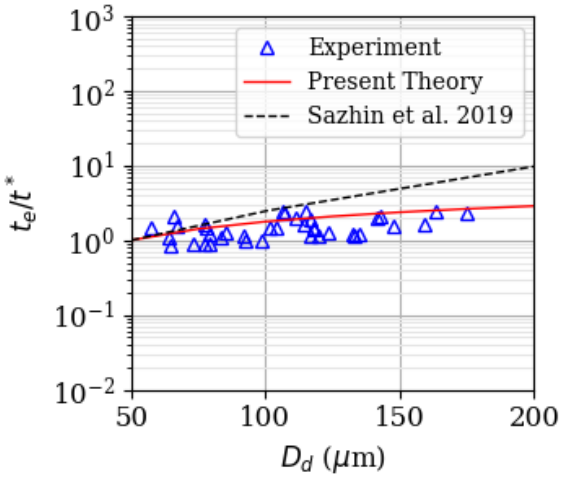

Figure 2: Comparison between normalized microexplosion delay times (t_e/t^*) predicted by the present theory (red solid line), experimental data (triangle markers) and theoretical prediction (black dash lines) from Sazhin et al. [25] for various initial droplet diameters.

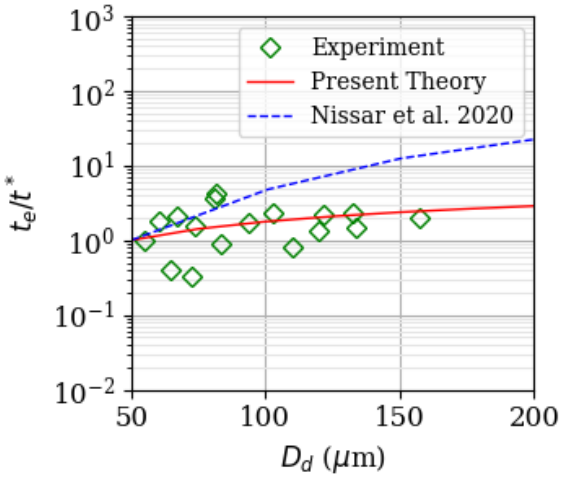

Figure 3: Comparison between normalized microexplosion delay times (t_e/t^*) predicted by the present theory (red solid line), experimental data (diamond markers) and theoretical prediction (blue dash lines) from Nissar et al. [26] for various initial droplet diameters.

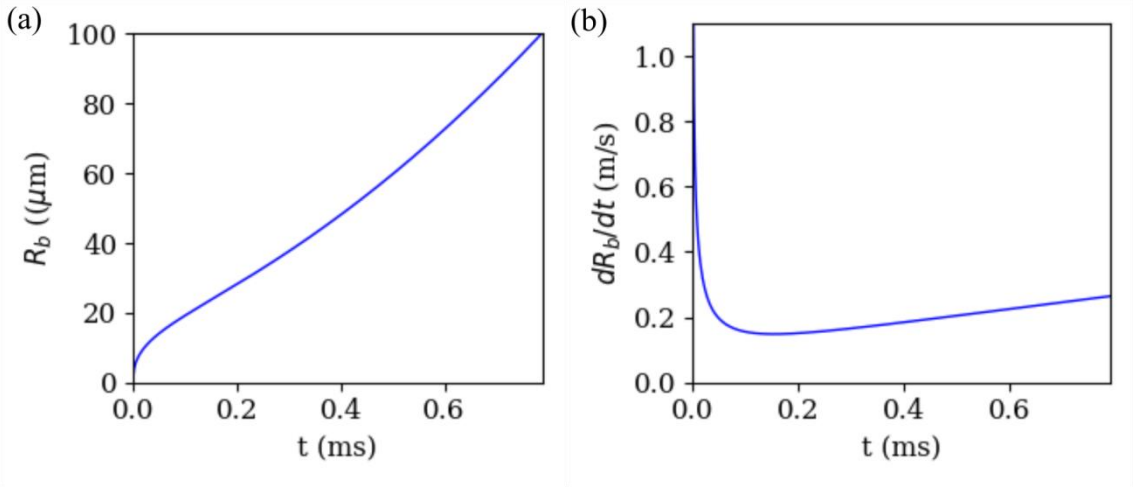

Figure 4: Variation of (a) bubble radius with time, and (b) bubble surface velocity with time.

The temporal evolution of the droplet radius is presented in Figure 5(a). It can be seen that the droplet radius increases nonlinearly with time, initially growing gradually until 0.2 ms, after which a sharp increase occurs. Although evaporation typically causes a decrease in droplet size, the growth of the bubble leads to an increase in the droplet radius. In the early stages (t < 0.2 ms), the small bubble has a minimal effect on droplet expansion, but its influence becomes significant at later stages. Figure 5(b) shows that the droplet surface growth rate increases almost linearly over time.

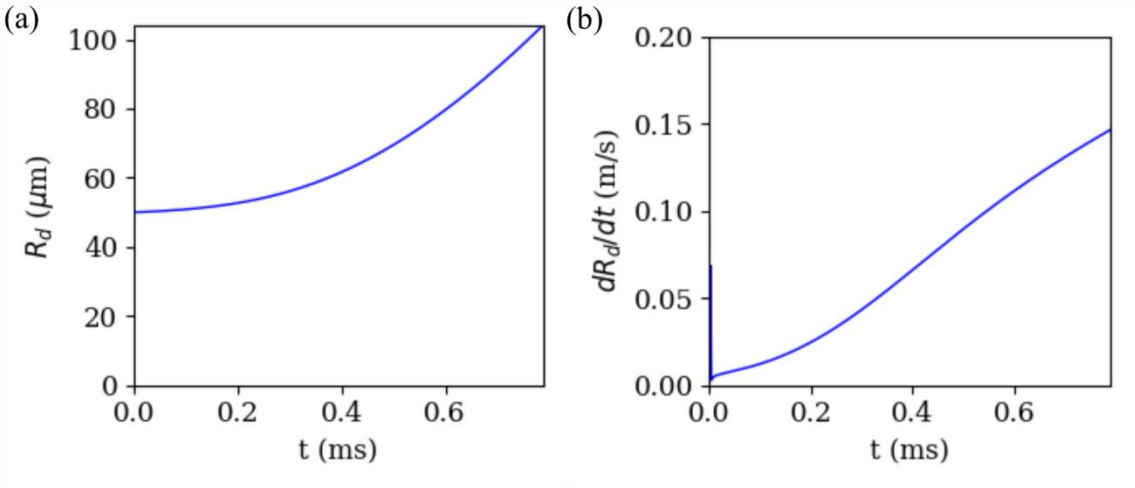

Figure 5: Variation of (a) droplet radius with time, and (b) droplet surface velocity with time.

Figure 6 illustrates the variation of bubble surface temperature over time, showing a rapid increase in the early stages followed by a more gradual rise. This trend indicates that there is limited heat transfer to the bubble during the later time periods, as there is little change in the bubble surface temperature. This phenomenon may be attributed to increased

evaporation at the droplet surface as the droplet size increases, which utilizes most of the heat supplied by the hot ambient environment.

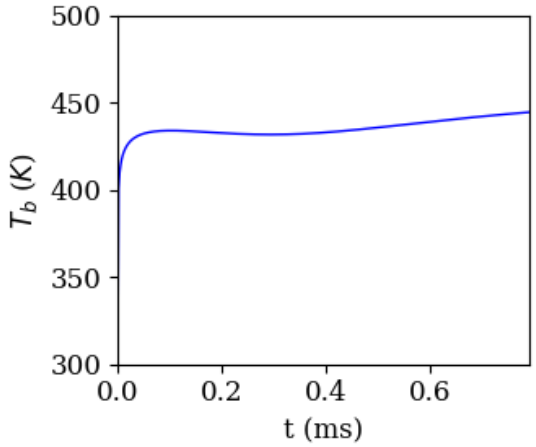

Figure 6: Variation of the bubble surface temperature with time.

4.3 Droplet Combustion

To demonstrate the capability of the developed model in capturing droplet combustion, we further analyzed the combustion of an n-dodecane droplet while neglecting bubble growth.

Figure 7(a) shows the surface regression of the droplet over scaled time, indicating that the square of the normalized droplet radius decreases linearly with time, consistent with the well-known d^2-law [40]. Figure 7(b) presents the variation of the mass evaporation rate over time, which decreases as time progresses, with a more rapid decline observed near droplet extinction. Additionally, Figure 7(c) shows that the flame moves closer to the droplet as the droplet surface regresses due to combustion. These results are consistent with previous studies of droplet combustions, which demonstrate the reliability of the developed model in this study to represent droplet combustion. The validation shown in Figure 7 serves two purposes: (i) To verify that when bubble growth is ignored in the proposed model, it reduces to the case of pure combustion, and (ii) To demonstrate that under normal combustion conditions, the droplet size decreases over time, whereas during a microexplosion in an emulsified droplet, the droplet size initially increases due to bubble growth.

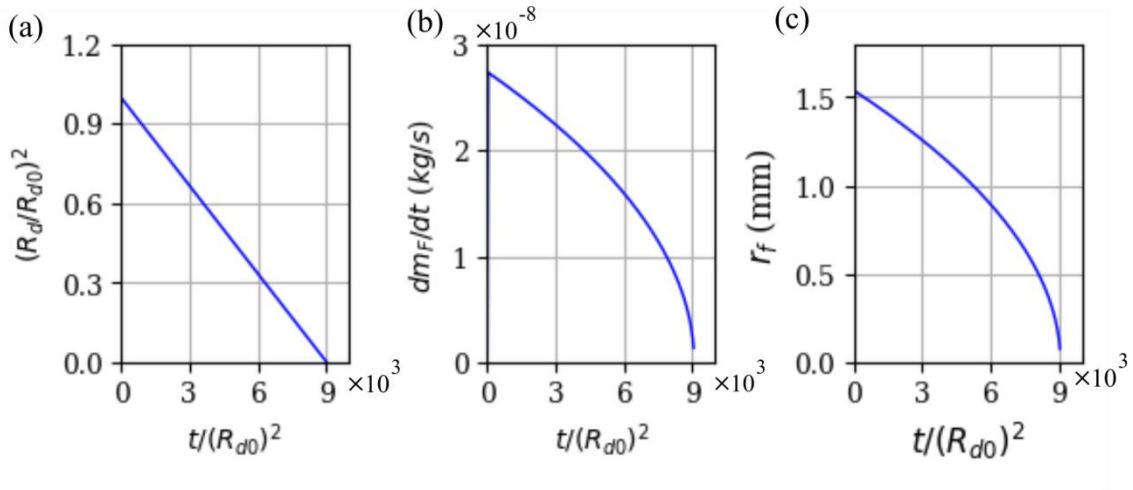

Figure 7: Combustion of n-dodecane droplet. (a) Surface regression of droplet with time, (b) variation of mass evaporation rate of the droplet with time, and (c) variation of flame location with time.

4.4 Microexplosion of combusting droplet

We further investigated the microexplosion of an n-dodecane/water droplet with a composition of 85%-15%, under combustion conditions. The droplet radius varies from 25 to 200 μm and the bubble radius varies in the rage of 1 to 5 μm.

Figure 8(a) shows the variation of the bubble radius over time within a droplet that has an initial radius of 50 μm. For a fixed initial bubble radius, the bubble radius increases steeply for a brief period during the early stages, after which it grows almost linearly with time. A similar behavior is observed under evaporation conditions as well, as shown in Figure 4(a). As the initial bubble radius increases, the bubble expands at a faster rate. However, the rate of bubble growth slows down as the bubble radius becomes larger. To further investigate this observation, the rate of change of the bubble radius (i.e., the bubble growth rate) is presented in Figure 8(b). It is noted that the droplet growth rate is similar for different initial bubble radii during the early period, where it declined sharply, after which it begins to increase slowly over time. It can also be observed that for larger initial bubble radii, the bubble growth is more pronounced, as indicated by the darker blue lines, consistent with earlier discussions.

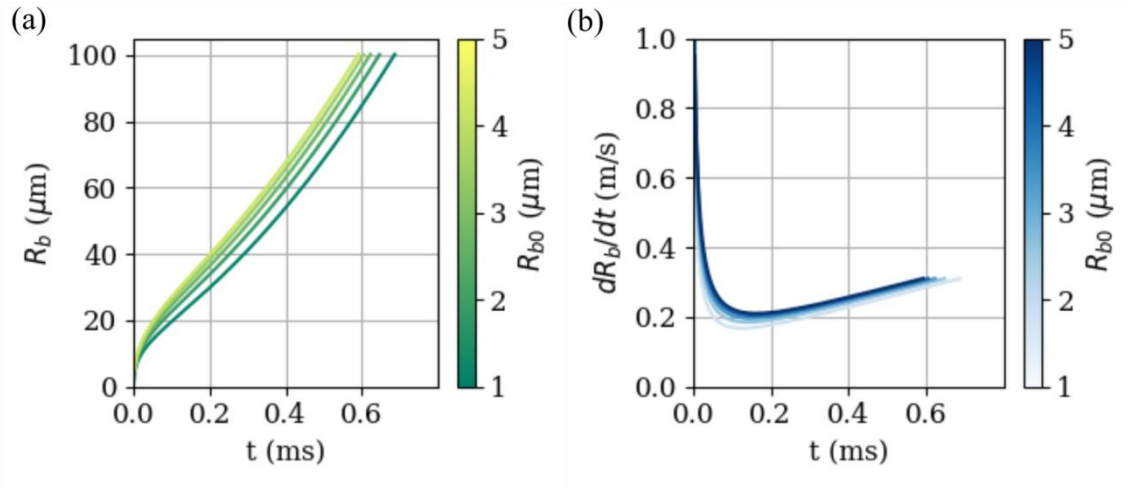

Figure 8: Variation of (a) bubble radius with time, and (b) bubble surface velocity with time (R_{d0} = 50 μm).

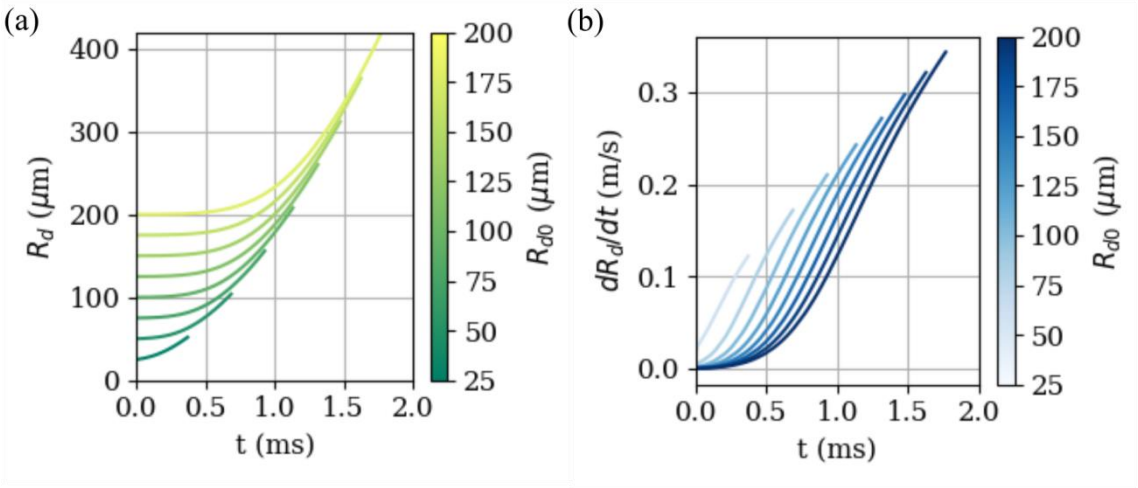

Figure 9: Variation of (a) droplet radius with time, and (b) droplet surface velocity with time (R_{b0} = 1 μm).

The droplet expansion behavior for different initial droplet radii while maintaining a fixed initial bubble radius is shown in Figure 9(a). Initially, the droplet radius remains constant, indicating that bubble growth has no effect on the droplet. However, in the later stages, the droplet radius begins to rise steadily. The presence of two distinct growth rate regions is more pronounced for larger initial droplet radii. In contrast, for the pure combustion case, the droplet radius decreases over time. Figure 9(b) presents the rate of change of the droplet radius (i.e., the droplet growth rate) for various initial droplet radii. It is observed that the droplet growth rate is zero at the beginning, followed by a monotonic

increase. The no-growth phase diminishes as the initial droplet radius decreases and completely disappears for smaller initial droplet radii.

Figure 10(a) further shows the variation of the flame location with time. It is interesting to note that the flame radius increases with time. In other hand, the flame radius decreases with time for pure combustion case as shown previously in Figure 7(c). The increase can be attributed to droplet expansion causing higher mass burning rate. To analyze the effect of heat transfer to the bubble surface, the bubble surface temperature is drawn in Figure 10(b). It is seen that the bubble surface temperature increase rapidly, then remain almost constant, and finally rises slowly. As in later time, most of the heat supplied to the droplet is used in phase change at the droplet surface, thus, there is smaller change is bubble temperature during this period. Therefore, the bubble growth is heat-controlled where the bubble growth rate declined sharply as discussed earlier (c.f. Figure 8(b)). In the later period, bubble growth is inertia-controlled, as there is little change in the bubble surface temperature. During this phase, both bubble growth and droplet growth rates are significantly high. This observation supports the existence of two distinct growth zones in the bubble growth diagram (see Figure 8(b)). Figure 10(c) displays the temperature contour in and around the droplet at several time instances. The location of the flame is indicated by a black dashed line. A zoomed-in view of the droplet region is also provided, allowing for a clearer observation of the bubble and droplet expansion. The zoomed-in view is scaled by a factor of 40. The droplet surface is illustrated by a green color line and the bubble surface by a black color line, while the white region in the center is the bubble. It is evident that both the bubble and droplet have expanded significantly from their initial sizes.

Figure 11 illustrates the relationship between microexplosion delay time and initial droplet radius for a fixed initial bubble radius. The microexplosion delay time increases with an increasing initial droplet radius, a trend that is similar to the evaporation case shown in Figure 2. It is evident that the increase in microexplosion delay time is nonlinear, with a faster rise observed for smaller initial droplet radii.

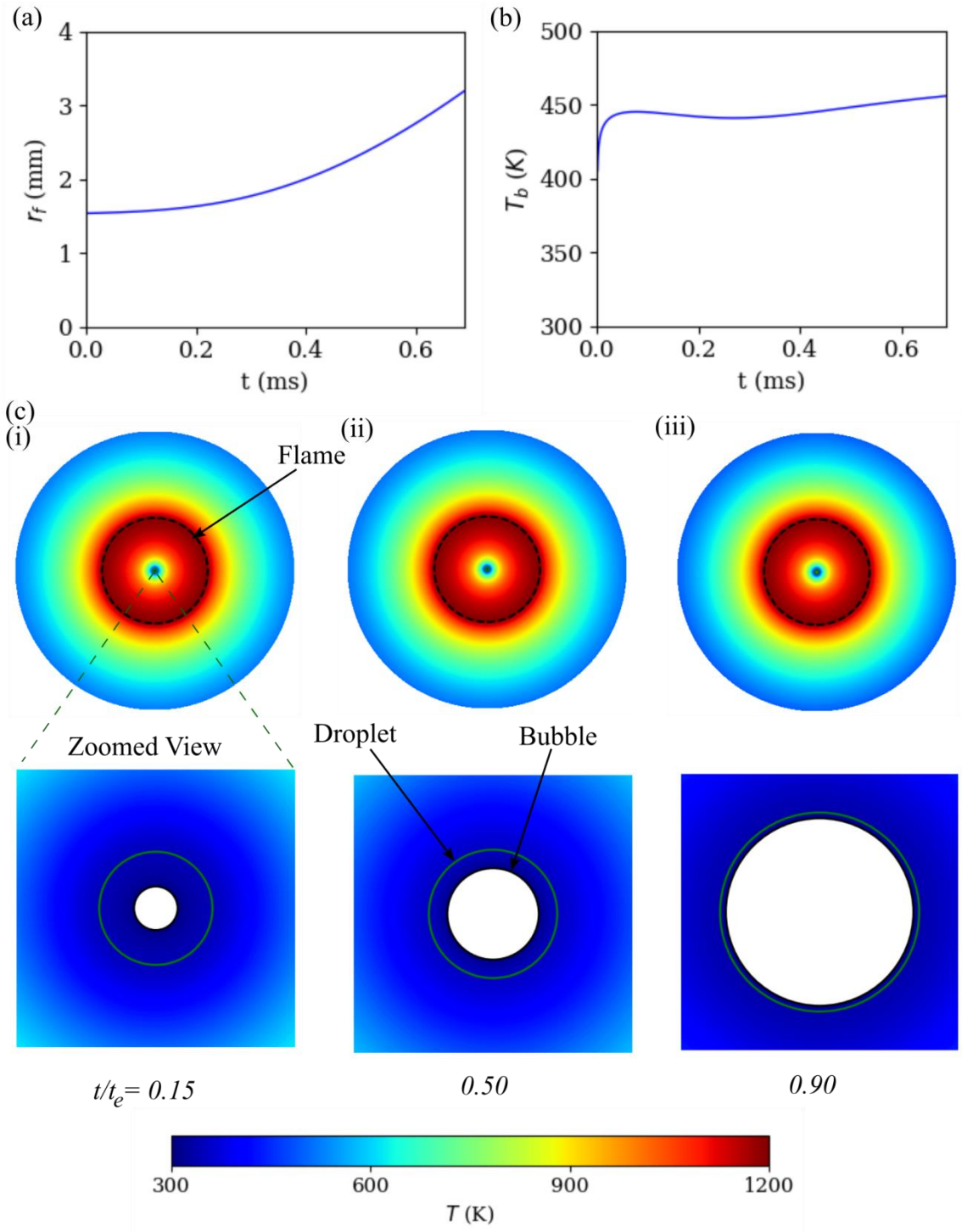

Figure 10: Variation of (a) flame radius with time, and (b) the bubble surface temperature with time. (c) Shows the bubble and droplet expansion and temperature contour in and around the droplet at several time instances (R_{d0} = 50 µm, R_{b0} = 1 µm).

Figure 12 presents the variation of microexplosion delay time with initial bubble radius while maintaining a constant initial droplet diameter. It is noted that the microexplosion delay time decreases gradually as the initial bubble radius increases. This

indicates that the microexplosion delay time is strongly dependent on droplet size and weakly dependent on bubble size, even though the bubble plays a significant role in causing the droplet to expand. A fivefold increase in bubble radius results in approximately a 15% deviation in the microexplosion delay time (see Fig. 11), whereas a fivefold increase in droplet radius leads to a much larger deviation of about 160% (see Fig. 12). Although, a bubble with an initial radius comparable to the droplet radius would result in a significantly different microexplosion delay time compared to a much smaller initial bubble. However, in practice, the bubble is formed through a nucleation process and typically has a size on the order of 1 μm. In contrast, droplets in sprays usually have radii ranging from 100 μm to 500 μm. Therefore, the chosen bubble and droplet size conditions in this study reflect those commonly observed in practical spray device applications.

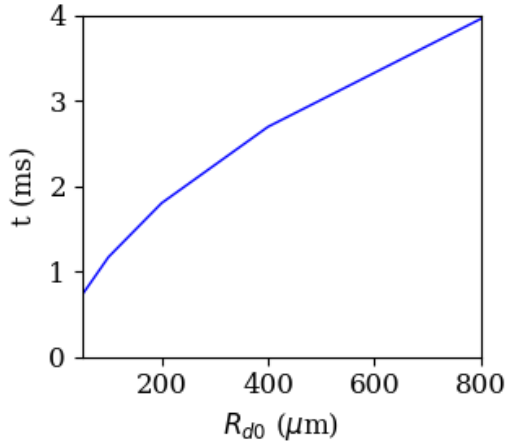

Figure 11: Variation of the microexplosion delay time with initial droplet radius (R_{b0} = 1 μm).

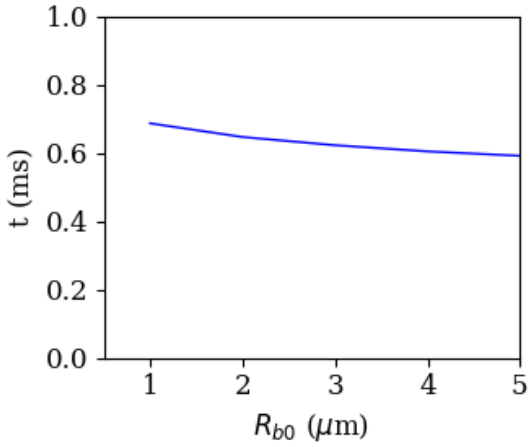

Figure 12: Variation of the microexplosion delay time with initial bubble radius (R_{d0} = 50 μm).

5. Conclusions

This paper presents an analytical model for microexplosions in burning droplets, incorporating bubble growth, heat transfer within the droplet, and droplet combustion. The sub-model for bubble growth, heat transfer, and combustion are integrated into a unified framework designed to provide a comprehensive understanding of microexplosion phenomena in burning emulsified fuel droplets.

Prior to applying the model to study microexplosions in burning droplets, the model is first validated under two scenarios: evaporation with microexplosions and pure droplet combustion without bubble growth, with a case study of n-dodecane/water droplets. These validations ensure the robustness and accuracy of the developed model. For evaporating droplets, microexplosion delay times are evaluated at various initial droplet diameters and compared with experimental data from the literature, showing commendable agreement. In the case of droplet combustion without bubble growth, the droplet radius regression follows the classical d^2-law, and the flame front moves closer to the droplet surface as the droplet size decreases.

The analytical model is further used to examine the evolution of key parameters prior to the onset of microexplosion, including the bubble radius, droplet radius, bubble surface temperature, and flame radius. The growth of the bubble radius exhibits two distinct stages: an initial thermally controlled stage followed by an inertially controlled stage. Similarly, droplet growth also progresses in two stages. In the first stage, droplet growth occurs independently of bubble growth, while in the second stage, their growth becomes interdependent. Interestingly, the intensity of microexplosion decreases gradually with an increase in the initial bubble radius, but increases sharply with a larger initial droplet radius. The flame radius is observed to increase over time due to significant droplet expansion. In contrast, it decreases when the effects of bubble and droplet expansion are neglected. Overall, the developed model demonstrates strong potential for application in practical spray combustion simulations, offering a good balance between computational efficiency and modeling fidelity.

Acknowledgement

This work is supported by Research seed fund at NIT Rourkela, India, and by the Research Grants Council of the Hong Kong Special Administrative Region, China, under No. 25104223 for the ECS project funded in 2023/24 Exercise.

References

[1] I. Glassman, R. A. Yetter, N. G. Glumac, Combustion, Academic Press, 2015.

[2] A. M. Attia, A. R. Kulchitskiy, Influence of the structure of water-in-fuel emulsion on diesel engine performance, Fuel 116 (2014) 703-708. https://doi.org/10.1016/j.fuel.2013.08.057

[3] O. A. Elsanusi, M. M. Roy, M. S. Sidhu, Experimental investigation on a diesel engine fueled by diesel-biodiesel blends and their emulsions at various engine operating conditions, Applied Energy 203 (2017) 582-593. https://doi.org/10.1016/j.apenergy.2017.06.052

[4] M. S. R. Dandu, K. Nanthagopal, B. Ashok, D. Balasubramanian, and R. Sakthivel, Impact of NOx control measures on engine life. NOx Emission Control Technologies in Stationary and Automotive Internal Combustion Engines, (2022) 387-421. https://doi.org/10.1016/B978-0-12-823955-1.00013-9

[5] H. Fayaz, M. A. Mujtaba, M. E. M. Soudagar, L. Razzaq, S. Nawaz, M. A. Nawaz, M. Farooq, A. Afzal, W. Ahmed, T. Y. Khan, S. Bashir, H. Yaqoob, A. I. EL-Seesy, S. Wageh, A. Al-Ghamdi, and A. Elfasakhany, Collective effect of ternary nano fuel blends on the diesel engine performance and emissions characteristics. Fuel 293 (2021) 120420. https://doi.org/10.1016/j.fuel.2021.120420

[6] A. M. Ithnin, W. J. Yahya, M. A. Ahmad, N. A. Ramlan, H. A. Kadir, N. A. C. Sidik, T. Koga, Emulsifier-free Water-in-Diesel emulsion fuel: Its stability behaviour, engine performance and exhaust emission, Fuel 215 (2018) 454-462. https://doi.org/10.1016/j.fuel.2017.11.061

[7] V. M. Ivanov, P. I. Nefedov, Experimental investigation of the combustion process of natural and emulsified liquid fuels, NASA TT F-258 (1965) 1-23.

[8] C. K. Law, Internal boiling and superheating in vaporizing multicomponent droplets, AIChE Journal 24(4) (1978) 626-632. https://doi.org/10.1002/aic.690240410

[9] C. H. Wang, X. Q. Liu, C. K. Law, Combustion and microexplosion of freely falling multicomponent droplets, Combustion and flame 56(2) (1984) 175-197. https://doi.org/10.1016/0010-2180(84)90036-1

[10] H. Z. Sheng, L. Chen, C. K. Wu, The droplet group micro-explosions in W/O diesel fuel emulsion sprays, SAE transactions (1995) 1534-1542. https://www.jstor.org/stable/44633318

[11] H. Watanabe, T. Harada, Y. Matsushita, H. Aoki, and T. Miura, The characteristics of puffing of the carbonated emulsified fuel, International journal of heat and mass transfer, 52(15-16) (2009) 3676-3684.
[12] Y. Morozumi, and Y. Saito, Effect of physical properties on microexplosion occurrence in water-in-oil emulsion droplets, Energy & fuels, 24(3) (2010) 1854-1859.
[13] E. Mura, R. Calabria, V. Califano, P. Massoli, J. Bellettre, Emulsion droplet micro-explosion: Analysis of two experimental approaches, Experimental Thermal and Fluid Science 56 (2014) 69-74.
[14] V. Califano, R. Calabria, P. Massoli, Experimental evaluation of the effect of emulsion stability on micro-explosion phenomena for water-in-oil emulsions, Fuel 117 (2014) 87-94.
[15] M. Y. Khan, Z. A. Abdul Karim, A. R. A. Aziz, M. R. Heikal, and C. Crua, Puffing and microexplosion behavior of water in pure diesel emulsion droplets during Leidenfrost effect. Combustion Science and Technology, 189(7) (2017) 1186-1197.
[16] D. C. K. Rao, S. Karmakar, and S. Basu, Atomization characteristics and instabilities in the combustion of multi-component fuel droplets with high volatility differential, Scientific reports, 7(1) (2017) 1-15.
[17] D. C. K. Rao, S. Karmakar, and S. Basu, Bubble dynamics and atomization mechanisms in burning multi-component droplets, Physics of Fluids, 30(6) (2018) 067101.
[18] M. M. Avulapati, T. Megaritis, J. Xia, L. Ganippa, Experimental understanding on the dynamics of micro-explosion and puffing in ternary emulsion droplets, Fuel 239 (2019) 1284-1292.
[19] M. F. B. Stodt, J. D. Groeneveld, L. Mädler, J. Kiefer, and U. Fritsching, Microexplosions of multicomponent drops in spray flames. Combustion and Flame, 240 (2022) 112043.
[20] Y. Zeng, C. F. Lee, Modeling droplet breakup processes under micro-explosion conditions, Proceedings of the Combustion Institute 31(2) (2007) 2185-2193.
[21] J. Shinjo, J. Xia, L. C. Ganippa, A. Megaritis, Physics of puffing and microexplosion of emulsion fuel droplets, Physics of Fluids 26(10) (2014) 103302.
[22] J. Shinjo, J. Xia, A. Megaritis, L. C. Ganippa, R. F. Cracknell, Modeling temperature distribution inside an emulsion fuel droplet under convective heating: a key to predicting microexplosion and puffing, Atomization and Sprays, 26(6) (2016) 551-558.
[23] J. Shinjo, J. Xia, Combustion characteristics of a single decane/ethanol emulsion droplet and a droplet group under puffing conditions, Proceedings of the Combustion Institute 36(2) (2017) 2513-2521.

[24] P. Guida, A. Ceschin, F. E. H. Pérez, H. G. Im, W. L. Roberts, Computationally-derived submodel for thermally-induced secondary atomization, International Journal of Heat and Mass Transfer 199 (2022) 123448. https://doi.org/10.1016/j.ijheatmasstransfer.2022.123448

[25] S. S. Sazhin, O. Rybdylova, C. Crua, M. Heikal, M. A. Ismael, Z. Nissar, A. R. B. Aziz, A simple model for puffing/micro-explosions in water-fuel emulsion droplets, International Journal of Heat and Mass Transfer 131 (2019) 815-821. https://doi.org/10.1016/j.ijheatmasstransfer.2018.11.065

[26] Z. Nissar, O. Rybdylova, S. S. Sazhin, M Heikal, A. R. B. Aziz, M. A. Ismael, A model for puffing/microexplosions in water/fuel emulsion droplets, International Journal of Heat and Mass Transfer 149 (2020) 119208. https://doi.org/10.1016/j.ijheatmasstransfer.2019.119208

[27] S. S. Sazhin, Processes in Composite Droplets. In Droplets and Sprays: Simple Models of Complex Processes, Springer, Cham 2022, 277-325.

[28] S. S. Sazhin, T. Bar-Kohany, Z. Nissar, D. Antonov, P. A. Strizhak, O. D. Rybdylova, A new approach to modelling micro-explosions in composite droplets, International Journal of Heat and Mass Transfer 161 (2020) 120238.

[29] D. V. Antonov, G. V. Kuznetsov, and P. A. Strizhak, P, The micro-explosive fragmentation criteria of two-liquid droplets, International Journal of Heat and Mass Transfer, 196 (2022), 123293.

[30] D. V. Antonov, R. M. Fedorenko, P. A. Strizhak, G. Castanet, S. S. Sazhin, Puffing/micro-explosion of two closely spaced composite droplets in tandem: Experimental results and modelling, International Journal of Heat and Mass Transfer 176 (2021) 121449.

[31] D. V. Antonov, R. S. Volkov, R. M. Fedorenko, P. A. Strizhak, G. Castanet, S. S. Sazhin, Temperature measurements in a string of three closely spaced droplets before the start of puffing/micro-explosion: Experimental results and modelling, International Journal of Heat and Mass Transfer 181 (2021) 121837.

[32] S. Ray, P. Zhang, S. Cheng, (2023). Mathematical modeling of puffing and microexplosion in emulsified fuel droplets containing several bubbles: A case study on n-dodecane/water droplet, Fuel 345 (2023), 128195.

[33] D. V. Antonov, R. M. Fedorenko, G. V. Kuznetsov, P. A. Strizhak, Modeling the micro-explosion of miscible and immiscible liquid droplets, Acta Astronautica 171 (2020) 69-82. https://doi.org/10.1016/j.actaastro.2020.02.040

[34] L. Rayleigh, On the pressure developed in a liquid during the collapse of a spherical cavity, The London, Edinburgh, and Dublin Philosophical Magazine and Journal of Science 34 (1917) 94–98. https://doi.org/10.1080/14786440808635681

[35] M. S. Plesset, S. A. Zwick, The growth of vapor bubbles in superheated liquids, Journal of applied physics 25(4) (1954) 493-500. https://doi.org/10.1063/1.1721668

[36] B. B. Mikic, W. M. Rohsenow, P. Griffith, On bubble growth rates, International Journal of Heat and Mass Transfer 13(4) (1970) 657-666. https://doi.org/10.1016/0017-9310 (70) 90040-2.

[37] R. C. Reid, J. M. Prausnitz, B. E. Poling, The properties of gases and liquids, fourth ed., McGraw-Hill Inc., New York, 1987.

[38] G. K. Batchelor, An introduction to fluid dynamics, Cambridge university press, 2000.

[39] D. W. Hahn, M. N. Ozisik, Heat Conduction, third ed., John Wiley & Sons, 2012.

[40] S. R. Turns, An introduction to combustion: Concepts and applications. Third edition, New York, NY, USA: McGraw-Hill Companies, 2012.